Journal of
Polymer Materials

Tech Science Press

https://doi.org/10.32604/jpm.2026.076617

ARTICLE

# Characterization of Cellulose Nanofibrils Prepared by Direct TEMPO-Mediated Oxidation of Coffee Grounds

**Yujie Zhang, Yankai Zhao, Zhuang Zhao, Mengmeng Shan, Bochen Xu, Haoquan Xue, Junxuan Xu, Fan Wu and Qiang He***

College of Mechanical Engineering, Jiamusi University, Jiamusi, China

*Corresponding Author: Qiang He. Email: heqiang4532@163.com

Received: 23 November 2025; Accepted: 20 January 2026; Published: 03 April 2026

**ABSTRACT:** This study presents a sustainable approach for the valorization of spent coffee grounds (CG) by converting them into carboxylated cellulose nanofibrils (CG-TCNF) via formic acid/hydrogen peroxide pretreatment followed by TEMPO/NaClO/$NaClO_2$-mediated oxidation. The pretreatment efficiently removed lignin, hemicellulose, and other non-cellulosic components, yielding purified cellulose (CG-C) with high crystallinity (CrI = 84%). Subsequent regioselective oxidation introduced carboxyl groups at the C6 position of cellulose chains, achieving a high carboxylate content of 1.4 mmol/g. The resulting CG-TCNF exhibited a well-dispersed nanofibrillar morphology with an average width of 3.57 nm and a high specific surface area of 265 $m^2/g$. Comprehensive characterization confirmed the successful oxidation and nanofibrillation: Fourier Transform Infaraed (FT-IR) Spectroscopy revealed the characteristic carboxylate absorption bands, X-ray Diffraction (XRD) showed preserved cellulose I structure with a slight reduction in crystallinity (CrI = 79.2%), and zeta potential measurements indicated good colloidal stability (−45.23 mV) in aqueous suspension. Thermal analysis demonstrated that the introduced carboxyl groups reduced the thermal stability of the nanofibrils compared to the precursor cellulose. This work establishes a novel route for directly transforming coffee grounds into functional nanocellulose, highlighting its potential as a sustainable feedstock for high-value nanomaterials.

**KEYWORDS:** Spent coffee grounds; formic acid/hydrogen peroxide; TEMPO/NaClO/$NaClO_2$; carboxylated; cellulose nanofibrils

## 1 Introduction

The escalating global demand for sustainable materials has intensified research into renewable alternatives to petroleum-based products [1,2]. Among natural biopolymers, cellulose stands out as the most abundant organic compound on Earth, constituting a major component of plant cell walls. This linear homopolysaccharide consists of β-(1→4)-linked D-glucose units, forming robust crystalline and amorphous regions through extensive hydrogen bonding [3,4]. Annual biosynthesis of cellulose exceeds 1.5 trillion tons, representing an immense renewable resource [5]. Recent advancements have enabled the disintegration of native cellulose into nanoscale dimensions, yielding materials collectively termed nanocellulose. These nanomaterials are typically categorized into three primary forms: cellulose nanofibrils (CNFs), characterized by their elongated, flexible structure; cellulose nanocrystals (CNCs), possessing high crystallinity and rod-like morphology; and bacterial nanocellulose (BNC), produced microbially with high purity [6–8]. Nanocellulose demonstrates exceptional properties including superior mechanical strength (elastic modulus ~150 GPa), high specific surface area (up to 500 $m^2/g$), biodegradability, and tunable surface chemistry,

making it suitable for diverse applications in nanocomposites [9], biomedical devices [10], filtration membranes [11], sustainable packaging [12] and tissue engineering [13].

The isolation of nanocellulose from lignocellulosic biomass presents significant technical challenges due to the complex hierarchical structure of plant cell walls, where cellulose microfibrils are embedded in a matrix of hemicellulose and lignin [14]. Conventional production methods encompass mechanical, chemical, and enzymatic approaches, each with distinct limitations. Mechanical techniques such as high-pressure homogenization, microfluidization, and ultrasonication can effectively fibrillate cellulose but often require substantial energy input (up to 5 kWh/kg) and may reduce crystallinity [15,16]. Acid hydrolysis techniques, typically employing sulfuric or hydrochloric acid, effectively isolate cellulose nanocrystals through the selective digestion of amorphous cellulose domains. However, this prevalent method presents notable drawbacks, including the production of significant quantities of chemical effluent. Furthermore, the process introduces charged surface groups that can subsequently compromise the thermal stability of the final material [17,18]. Enzymatic processes offer environmental advantages through specificity and mild conditions but suffer from slow reaction kinetics and high enzyme costs [19]. In contrast, catalytic oxidation using nitroxyl radicals, such as TEMPO, has emerged as a promising route for the selective surface modification of cellulose under mild, aqueous conditions. The TEMPO-mediated oxidation system (e.g., TEMPO/NaBr/NaClO or TEMPO/NaClO/$NaClO_2$) selectively converts the C6 primary hydroxyl groups on cellulose chains to carboxylate groups, introducing anionic surface charges that facilitate subsequent nanofibrillation through electrostatic repulsion and osmotic swelling. This method operates at room temperature, preserves the native cellulose I crystalline structure, and enables high degrees of functionalization with minimal depolymerization when conditions are carefully controlled, offering a more sustainable and efficient alternative to traditional chemical approaches. While wood pulp remains the predominant industrial source, increasing attention has turned to non-wood alternatives including agricultural residues (rice husk, sugarcane bagasse, Pineapple leaf) [20–23], industrial byproducts (brewery spent grains) [24,25], and food processing waste [26–28]. However, these feedstocks often present challenges related to compositional variability, seasonal availability, and requirement for intensive pretreatment, necessitating continued exploration of abundant, low-cost alternatives with consistent quality [29–31].

Spent coffee grounds, a ubiquitous byproduct of global coffee consumption, represent a largely untapped resource with immense potential for sustainable valorization [32]. With over 18 million tons generated annually from coffee brewing worldwide, the majority of CG is currently disposed of in landfills, where its decomposition contributes significantly to greenhouse gas emissions and environmental pollution [33]. In alignment with the principles of a circular economy and zero-waste initiatives, there is a growing imperative to repurpose this abundant agro-industrial residue into value-added products. Compositionally, CG contains 8%–15% cellulose, 30%–40% hemicellulose, and 20%–30% lignin, alongside residual oils, proteins, and phenolic compounds, making it a promising candidate for biorefinery applications. Recent studies have explored various pathways for CG valorization, including its use in bioenergy production, biocomposites, bioplastics, adsorbents, and food additives [34]. These efforts highlight the versatility of CG as a feedstock; however, the direct conversion of CG into functionalized nanocellulose remains underexplored. Compared to other agricultural residues, CG offers distinct advantages such as year-round availability, relatively uniform composition, and a pre-comminuted physical state, which reduces the energy required for preprocessing. Given the demonstrated efficacy of TEMPO-mediated systems in functionalizing and nanofibrillating cellulose from various sources, we hypothesize that this catalytic oxidation approach can be effectively applied to coffee grounds cellulose to produce carboxylated nanofibrils with tailored surface chemistry and colloidal stability. This study seeks to address this gap by developing a streamlined route for

transforming CG into carboxylated cellulose nanofibrils, thereby contributing to waste reduction and the creation of advanced nanomaterials.

This study presents a comprehensive investigation into the direct conversion of spent coffee grounds into carboxylated cellulose nanofibrils through an integrated approach combining formic acid/hydrogen peroxide pretreatment with TEMPO-mediated oxidation. The research employs TEMPO/NaClO/$NaClO_2$ as a catalytic oxidation system to selectively convert C6 primary hydroxyl groups to carboxyl moieties under aqueous conditions, facilitating subsequent nanofibrillation. The resulting CG-TCNF undergo thorough characterization using multiple analytical techniques: X-ray diffraction (XRD) to determine crystallinity index and crystal structure; Fourier-transform infrared spectroscopy (FTIR) to identify functional groups and chemical modifications; transmission electron microscopy (TEM) to examine morphology and dimensions; zeta potential measurements to assess colloidal stability; and thermogravimetric analysis (TGA) to evaluate thermal degradation behavior. The novelty of this work lies in the integrated and direct valorization of spent coffee grounds-an abundant and underutilized waste-into carboxylated cellulose nanofibrils with tailored surface functionality and preserved crystalline structure, offering a sustainable pathway for advanced nanocellulose production.

## 2 Materials and Methods

### *2.1 Materials*

Coffee Grounds are solid residues produced during the brewing or boiling process after coffee beans are ground. They are mainly composed of caffeine, tannic acid, cellulose, protein and other components. The coffee grounds used in this study were sourced from Lucky coffee shops in Jiamusi, Heilongjiang Province, China. Initial preparation involved rinsing the CG with deionized water until a neutral pH was achieved, followed by drying in an oven at 60°C for 12 h. The component content of dried coffee grounds was quantified using the nitric acid-ethanol method with two consecutive extractions for cellulose, Soxhlet extraction for lipids, the Kjeldahl method for protein, and muffle furnace incineration for ash, as detailed in Section 2.2.11. The component content of dried coffee grounds was quantified using the nitric acid-ethanol method with two consecutive extractions, as previously described [35]. The cellulose, lipid, protein, and ash content of coffee grounds used here are 11.72% ± 0.31%, 9.77% ± 1.02%, 10.89% ± 0.56% and 2.75% ± 0.31%, respectively. 2,2,6,6-tetramethylpiperidine nitrogen oxide (TEMPO, 98%) and Sodium hypochlorite (NaClO, 40%) were purchased from Xiya Chemical Reagent Co., LTD. (Shandong China). Sodium hydroxide (NaOH, >97%) and sodium chlorite ($NaClO_2$, 80%) were purchased from Sinopharm Chemical Reagent Co., Ltd. (Shanghai China). Formic acid (HCOOH, 99.5%) and Hydrogen peroxide ($H_2O_2$, 30%) were purchased from Wengjiang Chemical Reagent Co., Ltd. (Guangdong China). Milli-Q water and deionized water were used throughout the experiments. All chemicals are used without further purification.

### *2.2 Methods*

#### *2.2.1 Pre-Treatment of Coffee Grounds*

The treatment of coffee grounds involved formic acid and hydrogen peroxide combined in several distinct volume ratios. The mixture was subsequently heated to 80°C and stirred continuously at 500 rpm for four hours. In this formic acid/hydrogen peroxide system, reactive oxygen species, particularly hydroxyl radicals (HO•), are generated *in situ*. These highly oxidative species play a crucial role in selectively cleaving ether and ester linkages in lignin and degrading hemicellulose, thereby facilitating the removal of non-cellulosic components while preserving the cellulose backbone [36]. Following the initial reaction, the mixture was filtered to separate the supernatant. The remaining solid material was then transferred directly

into a reactor charged with a fresh mixture of formic acid and $H_2O_2$ in an identical volumetric ratio. A subsequent reaction was carried out in this reactor at 90°C for 2 h [37]. Upon completion, the product was filtered a second time to isolate the solid fraction. This solid residue underwent extensive washing with copious amounts of deionized water and was subsequently oven-dried at 60°C for 24 h. The aqueous phases collected from both filtration steps were combined and stored at 2°C–8°C for later analysis. The resulting cellulose-rich material, designated Coffee Grounds Cellulose (CG-C), was thoroughly rinsed with deionized water until the effluent reached a neutral pH and then dried to a constant mass in an oven.

### *2.2.2 TEMPO-Mediated Oxidation of Coffee Grounds Cellulose*

A sample of dried coffee grounds (1 g, dry weight basis) was dispersed in 100 mL of deionized water containing 0.016 g of TEMPO and 0.1 g of sodium chlorite. The oxidation reaction was initiated by adding sodium hypochlorite (NaClO) at a charge of 20 mmol per gram of dry substrate to the slurry under ambient conditions. The pH of the mixture was maintained at 5.0 for 2 h using a pH-stat apparatus by the continuous addition of 0.5 M NaOH. The resulting TEMPO-oxidized cellulose (designated CG-TCNF) was isolated by filtration, washed extensively with deionized water, and stored as a wet paste at 4°C for subsequent use. The yield of CG-TCNF was determined gravimetrically by comparing the dry mass before and after the oxidation treatment. The carboxylate and aldehyde group contents within the oxidized material were quantified via conductometric titration according to a reported method [38].

### *2.2.3 Nanofibrillation of Oxidized Cellulose via TEMPO-NaClO-$NaClO_2$*

CG-TCNF was redispersed in deionized water at a solids concentration of 0.1% (w/v). The pH of the suspension was adjusted to 10.0 using dilute NaOH to ensure the complete conversion of carboxylic acid groups to their sodium carboxylate form, thereby enhancing electrostatic repulsion. This suspension was then subjected to ultrasonication for 8 min. Following sonication, the supernatant, containing individualized cellulose nanofibrils, was collected for characterization by transmission electron microscopy (TEM).

### *2.2.4 X-ray Diffraction (XRD)*

X-ray diffraction (XRD) analysis was employed to monitor the evolution of material structure throughout each processing phase. Using a Bruker D2 PHASER diffractometer with Cu-Kα radiation ($\lambda$ = 0.15418 nm) operated at 30 kV and 10 mA, the obtained spectra enabled the determination of both crystallite dimensions and the crystallinity index. The dried samples were put on the quartz base, and scans were taken at a speed of 0.02° $min^{-1}$ over a 2θ range of 5°–40°. Duplicate XRD analyses were performed on each material. The XRD diffractograms were smoothed and analyzed with Xpert HighScore Plus (PANalytical Technologies Pvt. Ltd., Netherlands) software. The Gauss function in OriginPro 9.0.0 (64 bit) (OriginLab Corporation, USA) was used to fit the curve. The percentage of crystallinity (CrI) was calculated using Eq. (1) below based on the areas beneath the crystalline and amorphous peaks after baseline correction [39].

$$CrI(\%) = \frac{Ac}{Ac + Aa} \times 100\% \quad (1)$$

where $A_a$ and $A_c$ are the areas under the amorphous and the crystalline peaks, respectively.

### 2.2.5 Fourier Transform Infrared (FTIR) Spectroscopy

Fourier-transform infrared spectroscopy was performed using a Shimadzu IRTracer-100 spectrometer. Spectra were acquired in transmittance mode across a wavenumber range of 500 to 4000 $cm^{-1}$, averaging 32 scans at a resolution of 4 $cm^{-1}$. A background spectrum was collected and subtracted from all sample measurements prior to data analysis.

### 2.2.6 TEM Particle Size

The morphology of the cellulose nanofibril was examined using a JEOL JEM-1400F transmission electron microscope operated at an accelerating voltage of 100 kV. For imaging, a droplet of a 1.0 wt% cellulose nanofibrils suspension was deposited onto a copper grid and allowed to dry at room temperature. Observations were conducted in duplicate. The specific surface area (SSA) of the nanocrystals was estimated based on a cylindrical model using Eq. (2) [40]:

$$Specific\ surface\ area\left(SSA, m^2/g\right) = \frac{4}{\rho \cdot d} \tag{2}$$

where $\rho$ is the density of cellulose (1.5 g/$cm^3$) and d is the average diameter of an individual cellulose nanofibril.

### 2.2.7 Conductometric Titration

The carboxyl group content was determined via conductometric titration. Briefly, 0.1 g of CG-TCNF was dispersed in 100 mL of a 0.5 M NaCl aqueous solution under stirring. Subsequently, 5 mL of a 0.1 M HCl/0.5 M NaCl mixture was added. The suspension was titrated with a 0.1 M NaOH/0.5 M NaCl solution while monitoring the potential change using an automatic potentiometric titrator (ZD-2, Shanghai LeiCi). A plot of NaOH volume vs. $\Delta E^2/\Delta V^2$ was generated using a second-derivative method, with the inflection point indicating total NaOH consumption. The NaOH volume attributable to carboxyl groups was derived from this data. The carboxyl content ($C_{\text{-COOH}}$) was calculated in mmol/g using Eq. (3), where $V_{NaOH}$ and $V_{HCl}$ are the volumes (mL) of NaOH and HCl, respectively, $M_{NaOH}$ is the molarity of NaOH, and $W_{cellulose}$ is the dry mass of CG-TCNF used. The titration was performed in triplicate.

$$C_{-COOH} = \frac{\left(V_{NaOH} - V_{HCl}\right) * M_{NaOH}}{W_{cellulose}} \tag{3}$$

### 2.2.8 Zeta Potential (ζ) Measurements

Zeta potential value is one of the critical parameters which indicates the dispersity of the cellulose nanofibers. The zeta potential was measured using dynamic light scattering (Brookhaven Instruments) in phase analysis light scattering (PALS) mode. Samples were prepared as 0.01 wt% suspensions in double-distilled water (pH 7.0 ± 0.2, adjusted with 0.1 M NaOH/HCl; ionic strength < 0.1 mM) and equilibrated at 25°C for 10 min prior to analysis. Three replicates were performed per sample, with Smoluchowski's approximation applied for ζ calculation (ISO 13099-2:2012 Colloidal systems-Methods for zeta potential determination). To evaluate ionic strength effects, parallel measurements were conducted in NaCl solutions (1–150 mM, pH 7.0).

### 2.2.9 Thermogravimetric Analysis

Thermogravimetric analysis was employed to evaluate and compare the thermal decomposition profiles of materials from different treatment stages. Measurements were conducted using a METTLER TOLEDO

TGA/DTA 851e analyzer. For each run, a 2–4 mg sample was placed in a 70 μL aluminum crucible, which was hermetically sealed and then automatically perforated by the instrument immediately prior to analysis. A constant nitrogen purge of 40 mL $min^{-1}$ was maintained to provide an inert atmosphere. The temperature was increased at a constant rate of 10°C $min^{-1}$, and the resultant weight loss (TGA) and heat flow (DTA) were recorded as functions of temperature.

#### *2.2.10 Compositional Analysis*

The chemical composition of raw coffee grounds, including cellulose, lipid, protein, and ash content, was determined using the following standardized methods. Cellulose content was quantified using the nitric acid-ethanol method with two consecutive extractions, as previously described [41]. Lipid content was determined by Soxhlet extraction with petroleum ether (boiling range 40°C–60°C) as the solvent for 6 h, following AOAC Official Method 920.39. The protein content was calculated from the total nitrogen content measured using the Kjeldahl method (Kjeltec 8400 analyzer, FOSS, Denmark) according to AOAC Official Method 984.13, using a nitrogen-to-protein conversion factor of 6.25. Ash content was obtained by incinerating approximately 2 g of dried sample in a muffle furnace (SX2-4-10, Jingda, China) at 550°C for 5 h until constant weight, following AOAC Official Method 942.05. All determinations were performed in triplicate, and results are expressed as mean ± standard deviation on a dry weight basis.

#### *2.2.11 Statistical Analysis*

All tests were conducted in triplicate, and the results are presented as means ± standard deviations. Analysis of variance (ANOVA) was used to determine significant differences among the means at $p < 0.05$, using Duncan's multiple range test with Origin2022 software.

## 3 Results and Discussion

### *3.1 Morphological and Compositional Analysis of Coffee Grounds through Sequential Processing Stages*

During the sequential chemical treatments, the physical and chemical states of coffee grounds underwent significant transformations, reflecting the progressive removal of non-cellulosic components and the structural modification of cellulose. As illustrated in Fig. 1, the color of the raw coffee grounds transitioned from light brown to reddish-brown after formic acid and peroxyformic acid treatment, and finally to a clear white following bleaching. This visual evolution is indicative of the systematic elimination of lignin, hemicellulose, waxes, pectin, and other colored impurities.

Initially, the coffee grounds were subjected to an acidic environment with formic acid and hydrogen peroxide, which facilitated the partial dissolution of hemicellulose, waxes, and pectin. Under acidic conditions, the residual lignin swelled and migrated toward the fiber surface, enhancing its accessibility for subsequent oxidative cleavage [42]. The deepening of color to reddish-brown at this stage can be attributed to the migration and surface accumulation of phenolic derivatives in lignin, which strongly absorb visible light [43]. The peroxyformic acid system (generated *in situ* from formic acid and $H_2O_2$) played a critical role in delignification. As introduced in Section 2.2.1, the reactive oxygen species, particularly hydroxyl radicals (HO•), selectively attacked and fragmented the lignin polymer, breaking ether and ester linkages without significantly degrading the cellulose backbone. This step softened the fiber structure and removed a substantial portion of lignin, waxes, and pectin [44]. However, the lignin residues remained on the fiber surface, contributing to the darkened appearance. Therefore, a bleaching step was necessary to fully remove the residual lignin and expose the purified cellulose fibers. The resulting cellulose-rich material (CG-C)

retained a semi-crystalline structure, comprising both ordered crystalline regions and disordered amorphous domains [45].

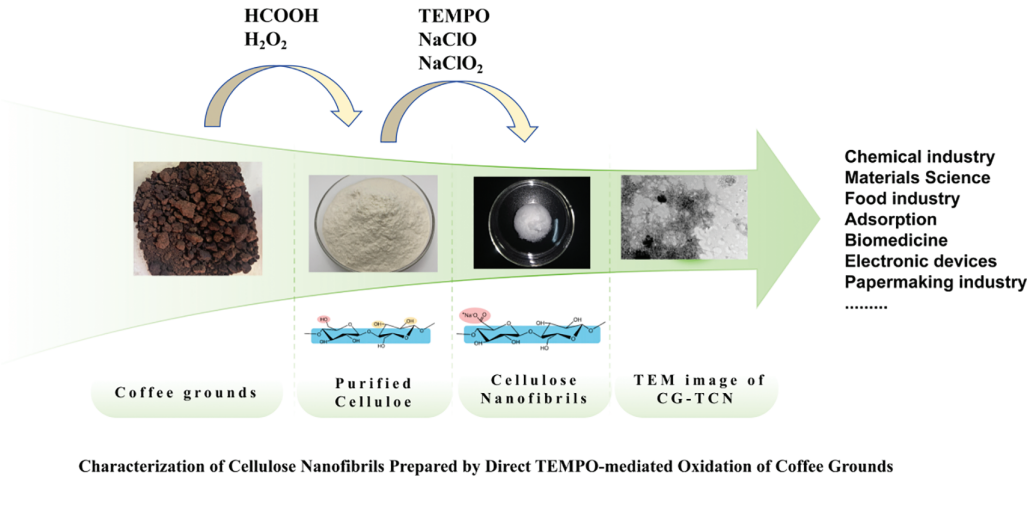


**Figure 1:** Coffee grounds photographs at various phases of chemical treatment.

The key nanofibrillation step employs the TEMPO/NaClO/$NaClO_2$ oxidation system, which selectively converts C6 primary hydroxyl groups of cellulose to carboxyl groups under aqueous, mild conditions. This regioselective oxidation introduces negative charges on the cellulose surface, promoting electrostatic repulsion between microfibrils [46]. During subsequent mechanical treatment (mild sonication), these oxidized cellulose fibers disintegrate into individualized nanofibril with uniform widths depending on raw material and processing intensity. The resulting CG-TCNF forms a stable, translucent hydrogel in water, indicating successful nanoscale dispersion and the presence of surface carboxylate groups, which enhance colloidal stability and interfacial reactivity. In summary, the sequential treatment-comprising formic acid/$H_2O_2$ delignification, bleaching and TEMPO-mediated oxidation-effectively transformed coarse coffee grounds into individualized, carboxylated cellulose nanofibrils with tailored surface chemistry and nanoscale dimensions.

### *3.2 X-ray Diffraction*

The X-ray diffractograms of the CG-C and the CG-TCNF are displayed in Fig. 2. Both materials retained the native cellulose Iβ crystalline allomorph, evidenced by characteristic diffraction signals at approximately 15.2°, 16.5°, and 22.6° (2θ), which are indexed to the (1–10), (110), and (200) lattice planes, respectively [47]. The purified cellulose (CG-C) showed a high crystallinity index (CrI) of 84%, which can be attributed to the effective removal of amorphous components such as lignin, hemicellulose, waxes, and pectins during the formic acid/peroxyformic acid pretreatment [48]. This treatment preserved the native crystalline arrangement of cellulose I, as evidenced by the sharp and symmetric diffraction peaks. In contrast, the CrI of CG-TCNF decreased to 79.2% after TEMPO-mediated oxidation. This reduction in crystallinity is primarily due to the selective oxidation of the C6 primary hydroxyl groups to carboxyl groups, which occurs preferentially on the surface and amorphous regions of cellulose microfibrils [49]. The oxidation process, involving the sequential conversion of hydroxyls to aldehydes and then to carboxyls, disrupts hydrogen bonding and partially erodes the crystalline domains, leading to a slight decrease in crystallinity without altering the cellulose I polymorphic structure [50].

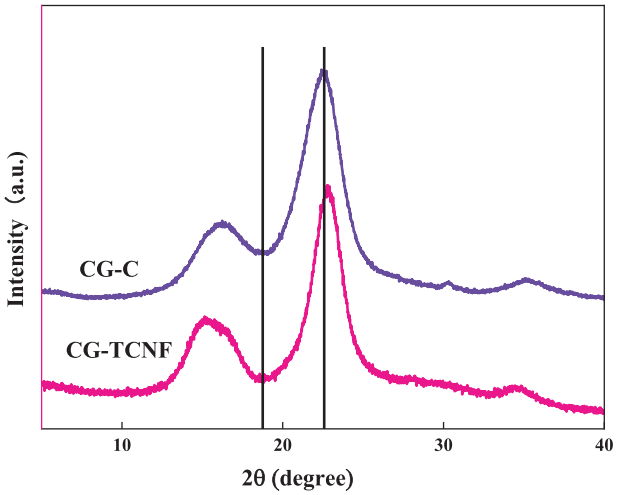


**Figure 2:** XRD patterns of CG-C and CG-TCNF.

The average crystallite size, estimated using Scherrer's equation based on the full width at half maximum (FWHM) of the (200) peak, also showed a slight decrease from CG-C to CG-TCNF, consistent with the partial disintegration of crystalline regions during oxidation [51]. This trend aligns with observations in other studies where TEMPO oxidation led to a moderate decline in crystallinity due to the introduction of carboxyl groups and subsequent mechanical disintegration into nanofibrils [52].

Compared to nanocellulose derived from other biomass sources, the CrI values of CG-TCNF (79.2%) are relatively high. For instance, TEMPO-oxidized cellulose nanofibers from rice husks exhibited CrI values around 42% [53], while those from bamboo dissolving pulp showed a CrI as low as 26.6% after NaOH/urea pretreatment and TEMPO oxidation [54]. The higher CrI in coffee grounds-derived CNF may be attributed to the mild oxidative conditions and the preservation of crystalline domains during the selective oxidation process. In contrast, more aggressive chemical or mechanical treatments in other biomass sources often result in greater disruption of crystalline order. Thus, the coffee grounds-based CNF combines high crystallinity with functional surface carboxylation, making it suitable for high-strength nanocomposites and functional materials.

### *3.3 FTIR Analysis*

The chemical structures of CG-C and CG-TCNF were investigated by FTIR spectroscopy, as shown in Fig. 3. Both samples exhibited characteristic cellulose absorption bands: a broad peak around 3340 $cm^{-1}$ attributed to O–H stretching vibrations, a signal at 2890 $cm^{-1}$ corresponding to C–H stretching [55,56]. And a prominent band at 1050 $cm^{-1}$ associated with C–O–C pyranose ring stretching [57,58]. The absence of peaks at 1730 $cm^{-1}$ (typical of unconjugated C=O in hemicellulose or lignin) and 1510 $cm^{-1}$ (aromatic skeletal vibrations from lignin) in CG-C confirms the effective removal of non-cellulosic components during the formic acid/$H_2O_2$ pretreatment [59].

After TEMPO-mediated oxidation, the spectrum of CG-TCNF revealed a new and distinct absorption band at approximately 1720 $cm^{-1}$, which is characteristic of the C=O stretching vibration of protonated carboxyl groups (–COOH) [60]. This peak provides direct evidence for the successful conversion of C6 primary hydroxyl groups to carboxyl groups via the TEMPO/NaClO/$NaClO_2$ oxidation system. The presence of this band, along with a concomitant increase in absorption near 1605 $cm^{-1}$ (assigned to the asymmetric stretching of $COO^-$ in the sodium carboxylate form), indicates that the oxidation introduced significant

anionic charge on the cellulose surface [61]. The coexistence of both protonated and deprotonated carboxyl species can be attributed to the sample preparation and the ionic environment during measurement.

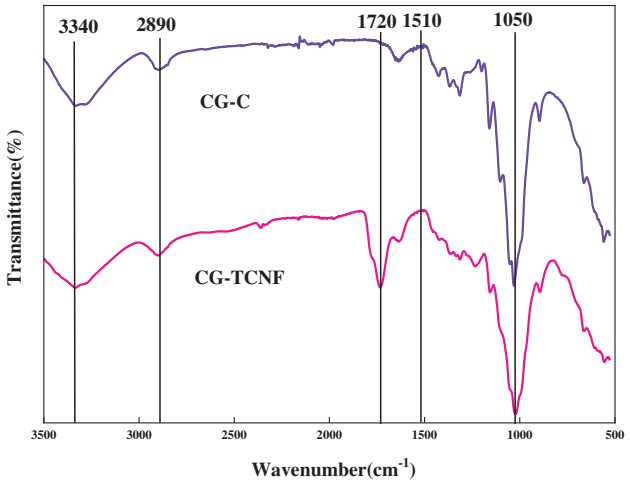


**Figure 3:** FTIR spectra recorded between 3500 and 500 $cm^{-1}$ of CG-C and CG-TCNF.

The intensity of the 1720 $cm^{-1}$ peak in CG-TCNF, compared to its absence in CG-C, underscores the high selectivity of the TEMPO system toward primary alcohols, leaving secondary hydroxyls and the cellulose backbone largely unaltered. This regioselective oxidation is crucial for imparting colloidal stability and facilitating nanofibrillation through electrostatic repulsion, without extensively degrading the cellulose crystalline core. The results align with previous studies on TEMPO-oxidized nanocelluloses from various lignocellulosic sources, where the emergence of the 1720 $cm^{-1}$ peak consistently signifies successful carboxylation, enabling subsequent functionalization and dispersion in aqueous media.

### *3.4 Morphological and Functional Group Content Analysis*

#### *3.4.1 Reaction Mechanism of TEMPO/NaClO/$NaClO_2$ Oxidation*

The oxidation of cellulose from coffee grounds was conducted using the TEMPO/NaClO/$NaClO_2$ catalytic system, which enables highly selective conversion of the C6 primary hydroxyl groups to carboxyl groups under mild aqueous conditions. As illustrated in Fig. 4, the reaction proceeds through a multi-step catalytic cycle involving the regeneration of the nitroxyl radical and the stepwise oxidation of cellulose hydroxyl groups. The mechanism begins with the oxidation of the stable nitroxyl radical TEMPO by NaClO to form the active N-oxoammonium ion ($TEMPO^+$). This cationic species selectively attacks the dissociated C6 primary hydroxyl groups on the cellulose chain, forming a covalent intermediate that rapidly decomposes to yield aldehyde groups and the reduced form of TEMPO, i.e., hydroxylamine (N-hydroxy-TEMPO) [62]. The regioselectivity toward primary alcohols-over secondary hydroxyls at C2 and C3-is attributed to the lower steric hindrance and higher accessibility of C6–OH, particularly under weakly acidic to neutral pH conditions where the dissociation of hydroxyl groups is favorable yet side reactions are minimized [63].

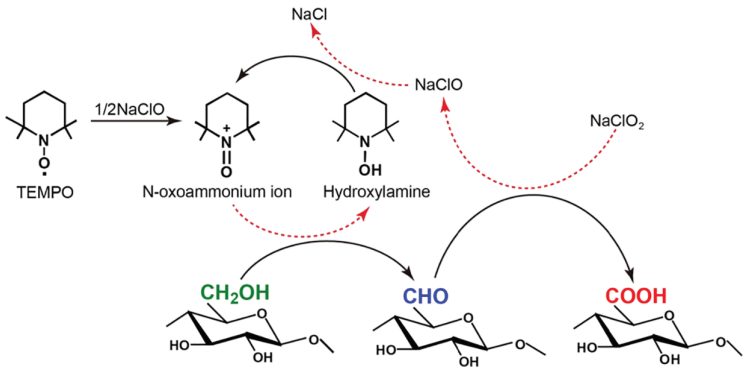


**Figure 4:** Schematic of the reaction mechanism of TEMPO/NaClO/$NaClO_2$ system in water.

In the subsequent step, the aldehyde intermediates are promptly oxidized to carboxyl groups by $NaClO_2$, which acts as the primary oxidant in the system [63]. This conversion proceeds through a hydrated aldehyde intermediate, which is further oxidized by $TEMPO^+$ or directly by $NaClO_2$, yielding sodium carboxylate groups on the cellulose surface. Notably, the presence of $NaClO_2$ effectively suppresses the accumulation of aldehyde groups, thereby mitigating undesirable side reactions such as β-elimination and depolymerization that commonly occur under alkaline conditions [64,65]. Simultaneously, the hydroxylamine species is reoxidized to $TEMPO^+$ by NaClO, closing the catalytic cycle and allowing TEMPO to participate in multiple turnover events. This regeneration step is crucial for maintaining high oxidation efficiency with only catalytic amounts of TEMPO. The overall stoichiometry results in the net consumption of $NaClO_2$, while NaClO and TEMPO function as catalysts [66]. The carboxylate content of CG-TCNF, measured at 1.4 mmol/g, reflects a high degree of surface functionalization. This is consistent with the proposed mechanism, wherein the oxidation occurs predominantly on the accessible surfaces of cellulose microfibrils-including both amorphous and crystalline regions-leading to the introduction of anionic charges that facilitate nanofibrillation through electrostatic repulsion and osmotic swelling. The mild reaction conditions (pH 5.0, room temperature) further help preserve the cellulose I crystalline structure, as confirmed by XRD results, while enabling efficient charge introduction. This mechanism aligns with previous studies on TEMPO-mediated oxidation of native celluloses, which emphasize the role of surface-limited reactions and the importance of controlling pH and oxidant ratios to balance between carboxylate introduction and cellulose degradation [67]. In the case of coffee grounds-derived cellulose, the successful nanofibrillation and high specific surface area (265 $m^2/g$) observed in CG-TCNF are direct outcomes of this regioselective and catalytic oxidation process.

### *3.4.2 Morphological Analysis by Transmission Electron Microscopy*

The morphology of the cellulose nanofibrils derived from coffee grounds was examined using TEM. As shown in Fig. 5a, the CG-TCNF samples exhibit a well-dispersed and interconnected network of nanofibrils with uniform width. Statistical analysis of the fibril dimensions (Fig. 5b) reveals an average width of 3.57 ± 1.39 nm and lengths extending to several hundred nanometers. The narrow size distribution suggests effective fibrillation and individualized nanofibril formation, attributable to the introduction of anionic carboxylate groups that promote electrostatic repulsion and swelling in aqueous media. Compared to the starting purified cellulose (CG-C), which retained a microfibrillar and fibrous structure, the TEMPO-mediated oxidation led to significant lateral disintegration into nanoscale fibrils, consistent with the behavior observed in wood-derived celluloses [68].

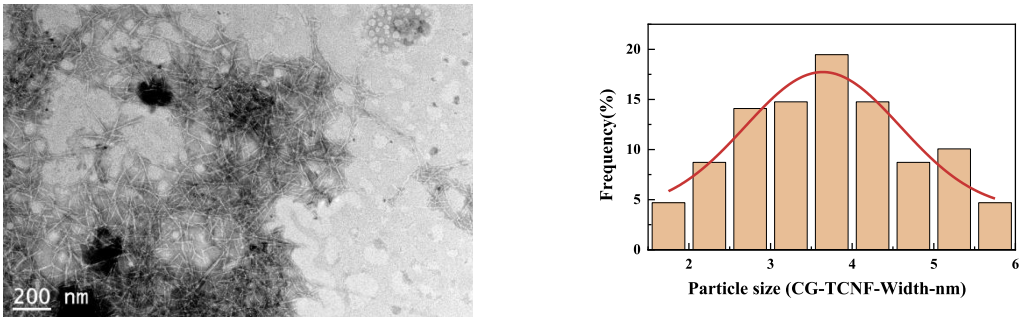


(**a**) (**b**)

**Figure 5:** TEM image (**a**) and particle size distribution curve (**b**) of cellulose nanofibrils (CG-TCNF).

*3.4.3 Specific Surface Area and Carboxyl Group Content*

The specific surface area of CG-TCNF was determined to be 265 $m^2/g$, a value significantly higher than that of the precursor CG-C, reflecting the successful nanofibrillation and increased accessibility of the fibrillar surfaces. This high surface area is conducive to applications requiring high reactivity or adsorption capacity.

Moreover, the carboxyl group content of 1.4 mmol/g, as measured by conductometric titration, confirms the successful and extensive surface functionalization via TEMPO-mediated oxidation. This high carboxylate density not only facilitates the individualization of fibrils through electrostatic and osmotic effects but also enhances the potential for further chemical modifications or interactions in composite materials. The correlation between high specific surface area and carboxyl content underscores the effectiveness of the TEMPO/NaClO/$NaClO_2$ system in producing nanofibrillated cellulose with both tailored morphology and surface chemistry.

### *3.5 Zeta Potential*

The colloidal stability and dispersion characteristics of the CG-TCNF was evaluated by zeta potential (ζ) measurements. The measured ζ value of CG-TCNF was −45.23 mV, indicating excellent electrostatic stabilization and a high degree of defibrillation in the aqueous suspension [69]. This negative potential arises primarily from the deprotonated carboxylate groups ($-COO^-$) introduced by the TEMPO/NaClO/$NaClO_2$ oxidation system, which imparts a net anionic charge to the fibril surfaces. According to classical DLVO theory, colloidal systems with $|\zeta| > 30$ mV are generally considered highly stable due to strong electrostatic repulsion, while values around $|\zeta| \approx 25–30$ mV suggest borderline stability, potentially leading to slow aggregation under certain conditions [70]. The observed value of −45.23 mV for CG-TCNF corroborates the carboxyl content of 1.4 mmol/g determined by conductometric titration, confirms that sufficient anionic charge was introduced to not only facilitate the initial nanofibrillation but also to maintain a well-dispersed state. The direct visual evidence from TEM imaging (Fig. 5a) supports this conclusion, showing a network of individualized nanofibrils without large aggregates. Furthermore, the high specific surface area (265 $m^2/g$) and uniform nanofibril morphology (average width 3.57 nm) enhance the accessibility of charged groups, contributing to the observed ζ potential. It is noteworthy that the ζ value close to −40 mV suggests that CG-TCNF suspensions remain dispersible under neutral or mildly alkaline conditions, though they may exhibit sensitivity to ionic strength or acidic environments where carboxyl groups become protonated, reducing electrostatic repulsion. This excellent dispersibility, stemming from the tailored surface chemistry, is a critical attribute for the subsequent processing and application of CG-TCNF in areas such as

nanocomposite fabrication, where uniform filler distribution is paramount, or in the formulation of stable gels and suspensions.

### *3.6 Thermal Analysis*

Thermogravimetric analysis (TGA) was employed to critically evaluate the thermal stability and decomposition kinetics of the purified cellulose (CG-C) and the resulting CG-TCNF. The thermal degradation profiles, as illustrated in Fig. 6, revealed significant changes following the nanofibrillation process. The CG-C exhibited robust thermal stability, with an initial decomposition temperature ($T_{onset}$) of 286°C and a maximum degradation temperature ($T_{max}$) of 376°C. In stark contrast, the CG-TCNF showed a substantially reduced thermal resilience, with a $T_{onset}$ of 222°C and a $T_{max}$ of 323°C.

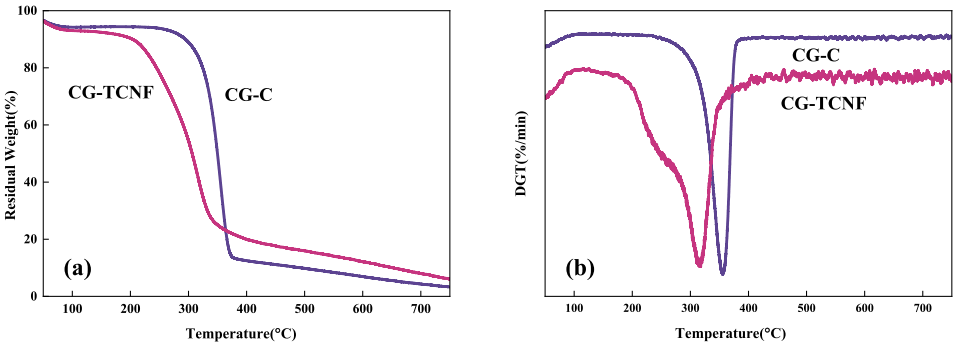


**Figure 6:** TGA curves (**a**) and DTG curves (**b**) of purified celluloses (CG-C) and cellulose nanofibrils (CG-TCNF).

The notable decrease of 64°C in the $T_{onset}$ for CG-TCNF can be attributed to a confluence of structural and chemical factors. Primarily, the TEMPO-mediated oxidation selectively converts the C6 primary hydroxyl groups into carboxyl groups, as confirmed by the FTIR and conductometric titration results. In aqueous dispersion, these groups deprotonate to form carboxylate anions ($–COO^-$), imparting a high negative surface charge, as evidenced by the ζ-potential of −45.23 mV. This anionic charge generates significant electrostatic repulsion between adjacent nanofibrils. This chemical modification disrupts the extensive inter- and intra-molecular hydrogen bonding network that is paramount to the structural integrity and thermal stability of native cellulose [71]. The repulsive forces actively work against the hydrogen bonding and van der Waals attractions that provide cohesion in native cellulose. The introduction of anionic carboxyl groups introduces electrostatic repulsion and weakens the cohesive energy between fibrils, thereby lowering the energy barrier required for the initiation of thermal degradation. This mechanism, where charged groups facilitate nanofibrillation via repulsion but concurrently reduce thermal stability, is consistent with the behavior of electrostatically stabilized nanocellulose systems reported in the literature [72,73]. Secondly, the nanofibrillation process, evidenced by TEM and specific surface area (SSA) calculations, results in a dramatic increase in surface area. This nanoscale dimension facilitates more efficient heat transfer to the reaction sites and provides a larger surface area for volatile release, effectively catalyzing the onset of decomposition. Furthermore, the XRD analysis indicated that the oxidation and subsequent ultrasonic treatment primarily affected the amorphous regions and the surfaces of the crystallites, leading to a relative increase in the accessibility of these less thermally stable domains. The combination of reduced crystallinity protection, heightened surface reactivity, and the introduction of thermally labile functional groups synergistically contributes to the earlier onset of weight loss in CG-TCNF.

The shift in the maximum degradation temperature ($T_{max}$) from 376°C to 323°C is a direct consequence of the altered pyrolysis pathway and the changed physical form of the material. In its microfibrous state,

CG-C degrades through a classic cellulose pyrolysis mechanism, involving depolymerization, transglycosylation, and the formation of levoglucosan, which is a relatively high-energy process. The compact, crystalline structure of CG-C necessitates higher temperatures for the scission of glycosidic bonds [74]. However, for CG-TCNF, the presence of carboxyl groups provides alternative, lower-energy decomposition pathways. Specifically, the carboxyl groups can undergo decarboxylation at elevated temperatures, releasing $CO_2$ and simultaneously creating radical sites that catalyze the further breakdown of the cellulose chain. This initiation step occurs at a lower energy threshold compared to the primary pyrolysis mechanisms (e.g., transglycosylation to levoglucosan) dominant in native cellulose. Furthermore, the acidic nature of these groups can catalyze dehydration reactions, steering the pyrolysis pathway towards lower-energy routes. This catalytic effect, combined with the structural destabilization caused by the disruption of the hydrogen-bonding network as previously discussed, synergistically lowers the overall thermal stability of the nanofibrils. These carboxyl groups can undergo decarboxylation reactions at elevated temperatures, releasing $CO_2$ and simultaneously creating radical sites on the cellulose backbone that accelerate the unzipping and fragmentation of the polymer chains [75]. Moreover, the extremely high surface area and the individualized nature of the nanofibrils mean that the primary volatile products, once formed, can escape the solid matrix much more readily, preventing secondary char-forming reactions and shifting the maximum rate of mass loss to a lower temperature [76]. This phenomenon is consistent with studies on nanocelluloses, where increased specific surface area is correlated with a lower $T_{max}$ [77].

To gain deeper insights into the pyrolysis behavior, the kinetic parameters were estimated using the Coats-Redfern model-fitting method, a widely adopted approach for solid-state thermal decomposition. The activation energy ($E_a$) for the main degradation stage was found to be lower for CG-TCNF compared to CG-C. This reduction in Ea aligns perfectly with the proposed structural model: the disrupted hydrogen-bonding network and the incorporation of carboxyl groups in CG-TCNF create a less thermally stable structure that requires less energy to decompose. The lower $E_a$ value for nanofibrillated cellulose, as opposed to its bulk counterpart, has been documented in other studies and underscores the trade-off between achieving nanoscale dispersion and functionalization at the expense of intrinsic thermal stability. In conclusion, the thermal analysis comprehensively demonstrates that the TEMPO oxidation and nanofibrillation process successfully functionalizes and individualizes the cellulose fibers but intrinsically alters their thermal degradation mechanism, leading to a material with lower decomposition temperatures and activation energy, a characteristic that must be considered for high-temperature processing and applications.

## 4 Conclusions

This study successfully demonstrates a direct and efficient pathway for valorizing spent coffee grounds into carboxylated cellulose nanofibrils through an integrated formic acid/hydrogen peroxide pretreatment followed by TEMPO/NaClO/$NaClO_2$-mediated oxidation. The pretreatment effectively removed non-cellulosic components, yielding purified cellulose with a high crystallinity index of 84%. Subsequent regioselective oxidation introduced carboxyl groups predominantly at the C6 position of cellulose chains, as unequivocally confirmed by the emergence of the characteristic FTIR band at 1720 $cm^{-1}$ and a high carboxylate content of 1.4 mmol/g. This surface functionalization was pivotal for the successful nanofibrillation, facilitating electrostatic repulsion that led to the disintegration of the oxidized fibers into individualized nanofibrils. The resulting CG-TCNF exhibited a well-dispersed, interconnected nanofibrillar network with an average width of 3.57 nm and a high specific surface area of 265 $m^2/g$. The introduced anionic charge also conferred a zeta potential of −45.23 mV, indicating excellent colloidal stability and dispersion characteristics in aqueous suspension. While the TEMPO oxidation slightly reduced the crystallinity index to 79.2%, the CG-TCNF retained the cellulose I allomorph and displayed a relatively high crystallinity compared to

nanocellulose from other agricultural residues. A trade-off between functionalization and thermal stability was observed, as the introduced carboxyl groups lowered the onset decomposition temperature, which is a recognized characteristic of TEMPO-oxidized nanocellulose. Overall, this work establishes a viable route for transforming an abundant agro-industrial waste into high-value, carboxylated nanofibrils with tailored surface chemistry and nanoscale dimensions, showcasing significant potential for applications in high-strength nanocomposites, responsive materials, and sustainable packaging.

**Acknowledgement:** The authors would like to thank the College of Mechanical Engineering, Jiamusi University.

**Funding Statement:** This research was funded by the training Program for College Students' Innovation and Entrepreneurship of Jiamusi University in Jiamusi City, Heilongjiang Province (grant number S202410222123).

**Author Contributions:** Yujie Zhang: investigation, data curation, writing-original draft, visualization, funding. Yankai Zhao: methodology, investigation. Zhuang Zhao: data curation, writing-original draft. Mengmeng Shan: data curation, writing—original draft. Bochen Xu: writing-original draft, visualization. Haoquan Xue: resources, supervision. Junxuan Xu: data curation, writing—original draft. Fan Wu: conceptualization, writing-original draft, supervision. Qiang He: conceptualization, writing—review & editing, supervision, funding. All authors reviewed and approved the final version of the manuscript.

**Availability of Data and Materials:** The data that support the findings of this study are available from the Corresponding Author upon reasonable request.

**Ethics Approval:** Not applicable.

**Conflicts of Interest:** The authors declare no conflicts of interest.

## References

1. Luo T, Hu Y, Zhang M, Jia P, Zhou Y. Recent advances of sustainable and recyclable polymer materials from renewable resources. Resour Chem Mater. 2025;4(2):100085. doi:10.1016/j.recm.2024.10.004.
2. Rajendran S, Al-Samydai A, Palani G, Trilaksana H, Sathish T, Giri J, et al. Replacement of petroleum based products with plant-based materials, green and sustainable energy—a review. Eng Rep. 2025;7(4):e70108. doi:10.1002/eng2.70108.
3. Picot-Allain MCN, Emmambux MN. Isolation, characterization, and application of nanocellulose from agro-industrial by-products: a review. Food Rev Int. 2023;39(2):941–69. doi:10.1080/87559129.2021.1928689.
4. Suzuki S, Horii F, Kurosu H. Theoretical investigations of $^{13}C$ chemical shifts in glucose, cellobiose, and native cellulose by quantum chemistry calculations. J Mol Struct. 2009;921(1–3):219–26. doi:10.1016/j.molstruc.2009.01.002.
5. Li X, Wan C, Tao T, Chai H, Huang Q, Chai Y, et al. An overview of the development status and applications of cellulose-based functional materials. Cellulose. 2024;31(1):61–99. doi:10.1007/s10570-023-05616-8.
6. Abbasi Moud A. Advanced cellulose nanocrystals (CNC) and cellulose nanofibrils (CNF) aerogels: bottom-up assembly perspective for production of adsorbents. Int J Biol Macromol. 2022;222(17):1–29. doi:10.1016/j.ijbiomac.2022.09.148.
7. Tofanica BM, Mikhailidi A, Fortună ME, Rotaru R, Ungureanu OC, Ungureanu E. Cellulose nanomaterials: characterization methods, isolation techniques, and strategies. Crystals. 2025;15(4):352. doi:10.3390/cryst15040352.
8. Hansini AMP, Galpaya GDCP, Gunasena MDKM, Abeysundara PM, Kirthika V, Bhagya L, et al. From nature to innovation: advances in nanocellulose extraction and its multifunctional applications. Molecules. 2025;30(13):2670. doi:10.3390/molecules30132670.
9. Reddy TRK, Jayaramudu T, Varaprasad K, Sani RK, Reddy GVS, Kim HJ. A review on nanocellulose in food packaging: a paradigm shift for enhanced mechanical strength and barrier performance. Int J Biol Macromol. 2025;322(2):146672. doi:10.1016/j.ijbiomac.2025.146672.

10. Zhao X, Zhang Y, Lv Z, Ding Z, Wang Y, Yang H, et al. Nanocellulose and its composites toward flexible supercapacitor. Adv Mater Technol. 2025;10(10):2401709. doi:10.1002/admt.202401709.
11. Khalid MY, Al Rashid A, Arif ZU, Ahmed W, Arshad H. Recent advances in nanocellulose-based different biomaterials: types, properties, and emerging applications. J Mater Res Technol. 2021;14(3):2601–23. doi:10.1016/j.jmrt.2021.07.128.
12. Mei B, Jiao P, Xie Y, Zhao Y, Li Y, Liu H. Wood derived conductive aerogel with ultrahigh specific surface area and exceptional mechanical flexibility for pressure sensing. Chem Eng J. 2024;500:157020. doi:10.1016/j.cej.2024.157020.
13. Asadnia M, Sadat-Shojai M. Recent perspective of synthesis and modification strategies of cellulose nanocrystals and cellulose nanofibrils and their beneficial impact in scaffold-based tissue engineering: a review. Int J Biol Macromol. 2025;293(2013):139409. doi:10.1016/j.ijbiomac.2024.139409.
14. Martínez-Sanz M, Gidley MJ, Gilbert EP. Application of X-ray and neutron small angle scattering techniques to study the hierarchical structure of plant cell walls: a review. Carbohydr Polym. 2015;125(2):120–34. doi:10.1016/j.carbpol.2015.02.010.
15. Wang Y, Wei X, Li J, Wang F, Wang Q, Zhang Y, et al. Homogeneous isolation of nanocellulose from *Eucalyptus* pulp by high pressure homogenization. Ind Crops Prod. 2017;104:237–41. doi:10.1016/j.indcrop.2017.04.032.
16. Malucelli LC, Matos M, Jordão C, Lomonaco D, Lacerda LG, Carvalho Filho MAS, et al. Influence of cellulose chemical pretreatment on energy consumption and viscosity of produced cellulose nanofibers (CNF) and mechanical properties of nanopaper. Cellulose. 2019;26(3):1667–81. doi:10.1007/s10570-018-2161-0.
17. Padhi S, Singh A, Orsat V, Routray W. Isolation and characterization of nanocellulose from jackfruit peel: a comparative analysis of organic and inorganic acid hydrolysis on structural, thermal, and rheological properties. Biomass Bioenergy. 2025;196(1):107716. doi:10.1016/j.biombioe.2025.107716.
18. Niu F, Li M, Huang Q, Zhang X, Pan W, Yang J, et al. The characteristic and dispersion stability of nanocellulose produced by mixed acid hydrolysis and ultrasonic assistance. Carbohydr Polym. 2017;165(6):197–204. doi:10.1016/j.carbpol.2017.02.048.
19. Olaiya NG, Oyekanmi AA, Hanafiah MM, Olugbade TO, Adeyeri MK, Olaiya FG. Enzyme-assisted extraction of nanocellulose from textile waste: a review on production technique and applications. Bioresour Technol Rep. 2022;19(8):101183. doi:10.1016/j.biteb.2022.101183.
20. Mandal A, Chakrabarty D. Isolation of nanocellulose from waste sugarcane bagasse (SCB) and its characterization. Carbohydr Polym. 2011;86(3):1291–9. doi:10.1016/j.carbpol.2011.06.030.
21. Scopel E, Pinto LO, Rezende CA. Residual lignin affectsproduction and properties of TEMPO-oxidized cellulose nanofibrils from partially delignified sugarcane bagasse. Cellulose. 2025;32(16):9315–31. doi:10.1007/s10570-025-06785-4.
22. Zhang W, Zhang M, Guan Q, Zhang X, Dong L, Ren S, et al. TEMPO-oxidized spent coffee grounds-derived cellulose nanofibers (TCCNs): physicochemical characterization and rheological properties. Cellulose. 2025;32(15):8917–38. doi:10.1007/s10570-025-06758-7.
23. Nguyen NTT, Phan-Huynh MA, Le Anh K, Van Hong Thien D, Hara K, Van-Pham DT. Pineapple leaf-derived TEMPO-oxidized cellulose nanospheres and graphene oxide composite: a green solution for ciprofloxacin adsorption. Cellulose. 2025;32(5):3317–34. doi:10.1007/s10570-025-06453-7.
24. Morales-Juárez AA, Terrazas Armendáriz LD, Alcocer-González JM, Chávez-Guerrero L. Potential of nanocellulose as a dietary fiber isolated from brewer's spent grain. Polymers. 2023;15(17):3613. doi:10.3390/polym15173613.
25. Bonfim KS, Morgado DL, Da Silva Fernandes R, Watanuki Filho A, Ahmad Aouada F, De Moura MR. Production and physicochemical characterization of TEMPO-oxidized bacterial cellulose nanofibers from industrial waste. Polímeros. 2025;35(4):e20250037. doi:10.1590/0104-1428.20240129.
26. Espinosa E, Rincón E, Morcillo-Martín R, Rabasco-Vílchez L, Rodríguez A. Orange peel waste biorefinery in multi-component cascade approach: polyphenolic compounds and nanocellulose for food packaging. Ind Crops Prod. 2022;187(2):115413. doi:10.1016/j.indcrop.2022.115413.

27. Hou G, Chitbanyong K, Shibata I, Isogai A. Can high-molar-mass cellulose molecules be extracted from phosphorylated pulp and TEMPO-oxidized pulps or their nanofibrils using LiCl/DMAc? Carbohydr Polym. 2025;367(3):124035. doi:10.1016/j.carbpol.2025.124035.
28. Jiang Y, Lu Y, Liu J, Zhao Y, Fan F. Characterization of bamboo shoot cellulose nanofibers modified by TEMPO oxidation and ball milling method and its application in W/O emulsion. LWT. 2024;205(2):116563. doi:10.1016/j.lwt.2024.116563.
29. Ono Y, Horikawa Y, Takeuchi M, Funada R, Isogai A. Distribution of carboxy groups in TEMPO-oxidized cellulose nanofibrils prepared from never-dried Japanese cedar holocellulose, Japanese cedar-callus, and bacterial cellulose. Cellulose. 2024;31(7):4231–45. doi:10.1007/s10570-024-05863-3.
30. Fakhrghasemi F, Shavisi N, Shahbazi Y, Yousefi H, Ullah A. Intelligent aerogels based on gelatin-sodium alginate containing tempo cellulose nanofibers and EncapsulatedEchinacea angustifoliaPetal extract into the kappa-carrageenan nanofibers to monitor the freshness of silver carp fillets. Food Bioprocess Technol. 2025;18(10):8861–79. doi:10.1007/s11947-025-03947-x.
31. Mazega A, Lehrhofer AF, Aguado RJ, Potthast A, Marquez R, Rosenau T, et al. Key insights into TEMPO-mediated oxidation of cellulose: influence of starting material. Cellulose. 2025;32(9):5227–46. doi:10.1007/s10570-025-06477-z.
32. Mekonnen BA, Fanta SW, De Greef J, Van Caneghem J, Vanierschot M. Torrefaction of spent coffee grounds for solid fuel production: a review. Fuel Process Technol. 2025;276(8):108280. doi:10.1016/j.fuproc.2025.108280.
33. Gebreeyessus GD. Towards the sustainable and circular bioeconomy: insights on spent coffee grounds valorization. Sci Total Environ. 2022;833:155113. doi:10.1016/j.scitotenv.2022.155113.
34. Dari DN, Da Silva LF, Júnior AMBL, Freitas IS, Da Silva Aires FI, Dos Santos JCS. Spent coffee grounds: insights and future prospects for bioenergy and circular economy applications. Green Technol Sustain. 2025;3(4):100213. doi:10.1016/j.grets.2025.100213.
35. Chen Q, Xiao S, Shi SQ, Cai L. Isolation of cellulose from poplar wood by nitric acid-ethanol treatment and its effect on the quality of films cast from ionic liquid. BioResources. 2018;13(4):8943–55. doi:10.15376/biores.13.4.8943-8955.
36. Rashidi O, Abdulkhani A, Hejazi S, Ashori A, Hosseinzadeh J, Sun F. Preparation and characterization of cellulose from wheat straw using formic/acetic acid pulping and Cu-activated hydrogen peroxide bleaching. Cellulose. 2025;32(1):165–85. doi:10.1007/s10570-024-06303-y.
37. Chang M, Wang X, Lin Q, Li R, Zhao L, Ren J, et al. Formic acid-hydrogen peroxide treatment of furfural residue for production of nanocellulose, lignin, and nano-scale lignin. Green Chem. 2022;24(16):6232–40. doi:10.1039/d2gc01211a.
38. Ostadi Moghadam M, Moeenfard M. How does particle size of spent coffee ground affect the physicochemical properties of isolated cellulose nanosphere? Results Chem. 2024;10(5):101683. doi:10.1016/j.rechem.2024.101683.
39. Segal L, Creely JJ, Martin AE Jr, Conrad CM. An empirical method for estimating the degree of crystallinity of native cellulose using the X-ray diffractometer. Text Res J. 1959;29(10):786–94. doi:10.1177/004051755902901003.
40. Serra A, González I, Oliver-Ortega H, Tarrès Q, Delgado-Aguilar M, Mutjé P. Reducing the amount of catalyst in TEMPO-oxidized cellulose nanofibers: effect on properties and cost. Polymers. 2017;9(11):557. doi:10.3390/polym9110557.
41. He Q, Bai Y, Lu Y, Cui B, Huang Z, Yang Q, et al. Isolation and characterization of cellulose nanocrystals from Chinese medicine residues. Biomass Convers Biorefin. 2024;14(21):27745–54. doi:10.1007/s13399-022-03380-6.
42. Vu AN, Nguyen LH, Tran HV, Yoshimura K, Tran TD, Van Le H, et al. Cellulose nanocrystals extracted from rice husk using the formic/peroxyformic acid process: isolation and structural characterization. RSC Adv. 2024;14(3):2048–60. doi:10.1039/d3ra06724f.
43. Hattori K, Arai A. Preparation and hydrolysis of water-stable amorphous cellulose. ACS Sustain Chem Eng. 2016;4(3):1180–6. doi:10.1021/acssuschemeng.5b01247.
44. Assonfack HL, Yona Cheumani AM, Ndinteh D, Lembe JT. Preparation and characterisation of cellulose by delignification of eteng (Ceiba pentandra) wood in formic acid-acetic acid-water solvent mixtures. J Polym Environ. 2023;31(3):913–21. doi:10.1007/s10924-022-02641-9.

45. Du J, Zhang X, Li X, Zhao J, Liu G, Gao B, et al. The cellulose binding region in *Trichoderma reesei* cellobiohydrolase I has a higher capacity in improving crystalline cellulose degradation than that of *Penicillium oxalicum*. Bioresour Technol. 2018;266(52):19–25. doi:10.1016/j.biortech.2018.06.050.
46. Tanaka R, Saito T, Isogai A. Cellulose nanofibrils prepared from softwood cellulose by TEMPO/NaClO/$NaClO_2$ systems in water at pH 4.8 or 6.8. Int J Biol Macromol. 2012;51(3):228–34. doi:10.1016/j.ijbiomac.2012.05.016.
47. Ureña-Benavides EE, Kitchens CL. Wide-angle X-ray diffraction of cellulose Nanocrystal–Alginate nanocomposite fibers. Macromolecules. 2011;44(9):3478–84. doi:10.1021/ma102731m.
48. Majdanac LD, Poleti D, Teodorovic MJ. Determination of the crystallinity of cellulose samples by X-ray diffraction. Acta Polym. 1991;42(8):351–7. doi:10.1002/actp.1991.010420802.
49. Qian R, Tang A, Chen G. TEMPO-mediated oxidation of cellulose and preparation of cellulose nanofibrils. J Biobased Mat Bioenergy. 2011;5(2):253–7. doi:10.1166/jbmb.2011.1145.
50. Driemeier C, Francisco LH. X-ray diffraction from faulted cellulose I constructed with mixed Iα–Iβ stacking. Cellulose. 2014;21(5):3161–9. doi:10.1007/s10570-014-0390-4.
51. Ju X, Bowden M, Brown EE, Zhang X. An improved X-ray diffraction method for cellulose crystallinity measurement. Carbohydr Polym. 2015;123(2):476–81. doi:10.1016/j.carbpol.2014.12.071.
52. Quintana E, Roncero MB, Vidal T, Valls C. Cellulose oxidation by laccase-TEMPO treatments. Carbohydr Polym. 2017;157(3):1488–95. doi:10.1016/j.carbpol.2016.11.033.
53. Fukuzumi H, Saito T, Iwata T, Kumamoto Y, Isogai A. Transparent and high gas barrier films of cellulose nanofibers prepared by TEMPO-mediated oxidation. Biomacromolecules. 2009;10(1):162–5. doi:10.1021/bm801065u.
54. Chen Y, Geng B, Ru J, Tong C, Liu H, Chen J. Comparative characteristics of TEMPO-oxidized cellulose nanofibers and resulting nanopapers from bamboo, softwood, and hardwood pulps. Cellulose. 2017;24(11):4831–44. doi:10.1007/s10570-017-1478-4.
55. Kotov N, Larsson PA, Jain K, Abitbol T, Cernescu A, Wågberg L, et al. Elucidating the fine-scale structural morphology of nanocellulose by nano infrared spectroscopy. Carbohydr Polym. 2023;302(1):120320. doi:10.1016/j.carbpol.2022.120320.
56. Hoseinpour Z, Niazmand R, Heydari-Majd M. Extraction and characterization of nanocellulose from *Cuminum cyminum* L. husk by ball-milling-assisted ultrasound. Carbohydr Polym Technol Appl. 2025;11(7):100934. doi:10.1016/j.carpta.2025.100934.
57. Kostryukov SG, Matyakubov HB, Masterova YY, Kozlov AS, Pryanichnikova MK, Pynenkov AA, et al. Determination of lignin, cellulose, and hemicellulose in plant materials by FTIR spectroscopy. J Anal Chem. 2023;78(6):718–27. doi:10.1134/S1061934823040093.
58. Ibrahim M, Osman O, Mahmoud AA. Spectroscopic analyses of cellulose and chitosan: FTIR and modeling approach. JNL Comp Theo Nano. 2011;8(1):117–23. doi:10.1166/jctn.2011.1668.
59. Hinterstoisser B, Akerholm M, Salmén L. Effect of fiber orientation in dynamic FTIR study on native cellulose. Carbohydr Res. 2001;334(1):27–37. doi:10.1016/s0008-6215(01)00167-7.
60. Hirota M, Tamura N, Saito T, Isogai A. Surface carboxylation of porous regenerated cellulose beads by 4-acetamide-TEMPO/NaClO/$NaClO_2$ system. Cellulose. 2009;16(5):841–51. doi:10.1007/s10570-009-9296-y.
61. Ono Y, Takeuchi M, Zhou Y, Isogai A. TEMPO/NaBr/NaClO and NaBr/NaClO oxidations of cotton linters and ramie cellulose samples. Cellulose. 2021;28(10):6035–49. doi:10.1007/s10570-021-03944-1.
62. Biliuta G, Fras L, Strnad S, Harabagiu V, Coseri S. Oxidation of cellulose fibers mediated by nonpersistent nitroxyl radicals. J Polym Sci Part A Polym Chem. 2010;48(21):4790–9. doi:10.1002/pola.24270.
63. Coseri S, Biliuta G, Zemljič LF, Srndovic JS, Larsson PT, Strnad S, et al. One-shot carboxylation of microcrystalline cellulose in the presence of nitroxyl radicals and sodium periodate. RSC Adv. 2015;5(104):85889–97. doi:10.1039/c5ra16183e.
64. Isogai A, Hänninen T, Fujisawa S, Saito T. Review: catalytic oxidation of cellulose with nitroxyl radicals under aqueous conditions. Prog Polym Sci. 2018;86:122–48. doi:10.1016/j.progpolymsci.2018.07.007.
65. Tang C, Chen H, Shi Z, Liu X, Liu L, Yu J, et al. Optimizing addition of NaClO in TEMPO-mediated oxidation of cellulose for less nanofiber degradation. Cellulose. 2024;31(18):10785–800. doi:10.1007/s10570-024-06262-4.

66. Ouhammou M, Mourak A, Ait-Karra A, Abderrahim J, Elhadiri N, Mahrouz M. Extraction, isolation, and TEMPO-NaBr-NaClO oxidation modification of cellulose from coffee grounds. Biomass. 2025;5(2):22. doi:10.3390/biomass5020022.
67. Kawamoto H, Saito S, Hatanaka W, Saka S. Catalytic pyrolysis of cellulose in sulfolane with some acidic catalysts. J Wood Sci. 2007;53(2):127–33. doi:10.1007/s10086-006-0835-y.
68. Saito T, Kimura S, Nishiyama Y, Isogai A. Cellulose nanofibers prepared by TEMPO-mediated oxidation of native cellulose. Biomacromolecules. 2007;8(8):2485–91. doi:10.1021/bm0703970.
69. Wei S, Liu X, Tao Y, Wang X, Lin Z, Zhang Y, et al. Strategy for enhanced soil lead passivation and mitigating lead toxicity to plants by biochar-based microbial agents. J Hazard Mater. 2025;489:137512. doi:10.1016/j.jhazmat.2025.137512.
70. He Q, Sun X, Bai Y, Meng X, Li C. Isolation of dicarboxy cellulose nanocrystal from spent fungi substrate and redispersion with gelatin. J Mol Liq. 2022;367(8):120397. doi:10.1016/j.molliq.2022.120397.
71. Debiagi P, Piazza V, Papagni M, Beretta A, Frassoldati A, Faravelli T. Cellulose pyrolysis kinetic model: detailed description of volatile species. Proc Combust Inst. 2024;40(1–4):105651. doi:10.1016/j.proci.2024.105651.
72. Yang H, Alam MN, Van De Ven TGM. Highly charged nanocrystalline cellulose and dicarboxylated cellulose from periodate and chlorite oxidized cellulose fibers. Cellulose. 2013;20(4):1865–75. doi:10.1007/s10570-013-9966-7.
73. Isogai A, Saito T, Fukuzumi H. TEMPO-oxidized cellulose nanofibers. Nanoscale. 2011;3(1):71–85. doi:10.1039/c0nr00583e.
74. Chen J, Lu Z, Cai J, Lin Y, Li Y, Yao S. Investigation of primary and secondary char formation during pyrolysis of torrefied cellulose. J Anal Appl Pyrolysis. 2025;191:107187. doi:10.1016/j.jaap.2025.107187.
75. Li K, Huang WZ, Yang SG, Yu JH, Niu Q, Zhao L, et al. Pretreatment-assisted catalytic pyrolysis for enhanced levoglucosenone production from waste cellulose acetate. J Anal Appl Pyrolysis. 2025;191(5):107234. doi:10.1016/j.jaap.2025.107234.
76. Zaritovskii AN, Kotenko EN, Grishchuk SV, Glazunova VA, Volkova GK. Studying catalytic synthesis of carbon nanostructures during microwave-assisted pyrolysis of cellulose. Phys Chem Asp Study Clust Nanostru. 2024;16:864–72. doi:10.26456/pcascnn/2024.16.864.
77. Zhang Y, Li Z, Zhou T, Jia G. Catalytic fast pyrolysis of cellulose to oxygenates: roles of homogeneous and heterogeneous catalysts. EES Catal. 2024;2(6):1238–46. doi:10.1039/d4ey00154k.